Global-Local Forward Models within Bayesian Inversion for Large Strain Fracturing in Porous Media

Nima Noii, Thomas Wick, and Amirreza Khodadadian

1 Introduction

Phase-field fracture models are employed to capture failure and cracks in structures, alloys, and poroelastic media. The coupled model is based on solving the elasticity equation and an Allen-Cahn-type phase-field equation. In hydraulic fracture, a Darcy-type equation is solved to capture the pressure profile. Solving this coupled system of equations is computationally expensive. Indeed, to provide an accurate estimation (compared to the measurement) a very fine mesh profile is required. Of course, the time-dependent and nonlinear nature of the problem gives rise to more complexity. Another challenge is related to the computational, mechanical, and geomechanical material parameters. They have an essential effect on the simulations; however, many of them can not be estimated experimentally.

In [11], we used the Bayesian inversion to identify the parameters based on hydraulic fractures of porous media. A fracture response is realized through a phase-field equation [2] (based on the seminal work [3]). But that work is limited to small deformations. In the current study, we extend [11] towards a *large strain* formulation [1, 7].

In consequence, the main objective is to utilize non-intrusive global-local models [4] that are originally based on non-overlapping domain decomposition [12] to significantly reduce the computational cost in Bayesian inversion. In extension to our prior work, we introduce an adoption of the hydraulic phase-field fracture formulation of a material that undergoes large deformation in poroelastic media. Finally, ensemble Kalman filters are employed for the proposal adaption in Bayesian inversion to identify the mechanical material parameters once the multiscale approach is used to solve the forward model.

2 Framework for failure mechanics in hydraulic fracture

Let us assume $\mathcal{B} \subset \mathbb{R}^{\delta}$ is the solid computational domain (here $\delta = 2$) with its surface boundary $\partial\mathcal{B}$ and time $t \in \mathcal{T} = [0, T]$. The given boundary-value problem (BVP)

Thomas Wick, Amirreza Khodadadian
Leibniz University Hannover, Institute of Applied Mathematics and Cluster of Excellence PhoenixD, Welfengarten 1, 30167 Hannover, Germany,
e-mail: {thomas.wick,khodadadian}@ifam.uni-hannover.de
Nima Noii
Leibniz University Hannover, Institute of Continuum Mechanics, An der Universität 1, 30823 Garbsen, Germany e-mail: noii@ikm.uni-hannover.de

is a coupled multi-field system for the fluid-saturated porous media of the fracturing material. Since we are dealing in large strain setting, it is required to define the mapping between the referential position $\mathbf{X}$ towards spatial description $\mathbf{x}$ based on the motion $\boldsymbol{\varphi}$ of point P at time t, see Figure 1. The media can be formulated based on a coupled three-field system. At material points $\mathbf{x} \in \mathcal{B}$ and time $t \in \mathcal{T}$, the BVP solution indicates the deformation field $\boldsymbol{\varphi}(\mathbf{x}, t)$ of the solid, the fluid pressure field $p(\mathbf{x}, t)$, and the phase-field fracture variable d can be represented by

$$\boldsymbol{\varphi}\colon \begin{cases} \mathcal{B}\times\mathcal{T} \to \mathcal{R}^{\delta} \\ (\mathbf{X}, t) \mapsto \mathbf{x} = \boldsymbol{\varphi}(\mathbf{X}, t) \end{cases} \quad p\colon \begin{cases} \mathcal{B}\times\mathcal{T} \to \mathcal{R} \\ (\mathbf{X}, t) \mapsto p(\mathbf{X}, t) \end{cases} \quad d\colon \begin{cases} \mathcal{B}\times\mathcal{T} \to [0,1] \\ (\mathbf{X}, t) \mapsto d(\mathbf{X}, t) \end{cases} \tag{1}$$

Here, $d(\mathbf{x}, t) = 0$ and $d(\mathbf{x}, t) = 1$ are referred to as the unfractured and completely fractured parts of the material, respectively. The coupled BVP is formulated through three specific primary fields to illustrate the hydro-poro-elasticity of fluid-saturated porous media by

$$\text{Global Primary Fields}\colon \mathfrak{U} := \{\boldsymbol{\varphi}, p, d\}. \tag{2}$$

2.1 Elastic contribution

The elastic density function is formulated through a Neo-Hookean strain energy function for a compressible isotropic elastic solid

$$W_{\text{elas}}(\mathbf{F}, d) = g(d)\, \psi_{\text{elas}}(\mathbf{F}) \quad \text{with} \quad \psi_{\text{elas}}(\mathbf{F}) = \frac{\mu}{2}\left[(\mathbf{F}:\mathbf{F} - 3) + \frac{2}{\beta}(J^{-\beta} - 1)\right], \tag{3}$$

such that the shear modulus μ and the parameter $\beta := \beta(\nu) = 2\nu/(1-2\nu)$ with the Poisson number $\nu < 0.5$ are used. Here, the material deformation gradient of the solid denoted by $\mathbf{F}(\mathbf{X}) := \nabla\boldsymbol{\varphi}(\mathbf{X}, t) = \text{Grad}\boldsymbol{\varphi}$ with the Jacobian $J := \det[\mathbf{F}] > 0$ augmented with the symmetric right Cauchy-Green tensor $\mathbf{C} = \mathbf{F}^T\mathbf{F}$ is used; for details the reader is referred to [1, 11]. We note that the quadratic function $g(d) = (1-d)^2 + \kappa$ is denoted as a degradation function, with $\kappa \approx 10^{-8}$ that is chosen as a sufficiently small quantity. According to the classical Terzaghi theorem, the constitutive modeling results in the additive split of the stress tensor $\mathbf{P}$ to effective mechanical contribution and fluid part as

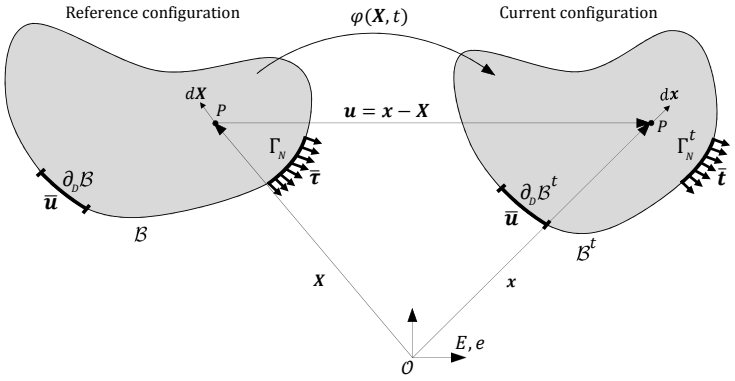

Fig. 1 Setup of the notation for the configuration and motion of the continuum body $\boldsymbol{\varphi}(\mathbf{X}, t)$. The initial position $\mathbf{X}$ in the undeformed configuration $\mathcal{B}$ toward the current position $\mathbf{x}$ in the spatial configuration $\mathcal{B}^t$ for the solid material undergoing finite strain.

$$\mathbf{P}(\mathbf{F}, p, d) := \frac{\partial W_{\text{elas}}}{\partial \mathbf{F}} = g(d)\mathbf{P}_{eff}(\mathbf{F}) - BpJ\mathbf{F}^{-T} \quad \text{with} \quad \mathbf{P}_{eff} = \mu\left[\mathbf{F} - J^{-\beta}\mathbf{F}^{-T}\right]. \tag{4}$$

Here, the first Piola-Kirchoff stress tensor $\mathbf{P}$ is derived from the first-order derivative of the pseudo-energy density function W_{elas} given in (3). Thus, the balance of linear momentum for the multi-field system prescribed through body force $\overline{\mathbf{b}}$ reads

$$\boxed{\text{Div}\,\mathbf{P}(\mathbf{F}, p, d) + \overline{\mathbf{b}} = \boldsymbol{0}.} \tag{5}$$

2.1.1 Fluid contribution

The fluid volume flux vector $\mathcal{F}$ is described through the negative direction of the gradient of the fluid pressure ∇p and permeability based on Darcy-type fluid's

$$\mathcal{F} := -\mathbf{K}(\mathbf{F}, d)\ \nabla p. \tag{6}$$

Here, the second-order permeability tensor $\mathbf{K}(\mathbf{F}, d)$, following [7], is additively decomposed into the permeability tensor into a Darcy-type flow for the unfractured porous medium $\boldsymbol{K}_{Darcy}$ and Poiseuille-type flow in a completely fractured material $\boldsymbol{K}_{frac}$ by

$$\begin{aligned} \boldsymbol{K}(\mathbf{F}, d) &= \boldsymbol{K}_{\text{Darcy}}(\mathbf{F}) + d^{\zeta}\boldsymbol{K}_{\text{frac}}(\mathbf{F}), \\ \boldsymbol{K}_{\text{Darcy}}(\mathbf{F}) &= \tfrac{K}{\eta_F} J\mathbf{C}^{-1}, \\ \boldsymbol{K}_{\text{frac}}(\mathbf{F}) &= K_c\ \omega^2\ J\left[\mathbf{C}^{-1} - \mathbf{C}^{-1}\mathbf{N} \otimes \mathbf{C}^{-1}\mathbf{N}\right]. \end{aligned} \tag{7}$$

Here, K_D is the isotropic intrinsic permeability of the pore space, K_c is the spatial permeability in the fracture, η_F is the dynamic fluid viscosity, and $\zeta \geq 1$ is a permeability transition exponent. Following [7], the so-called crack aperture (or the crack opening deformation) defined through $\omega = (\lambda_{\perp} - 1)h_e$ in terms of the stretch orthogonal to the crack surface $\lambda_{\perp}^2 = \nabla d \cdot \nabla d / \nabla d \cdot \mathbf{C}^{-1} \cdot \nabla d$ and the characteristic element length h_e. Also, $\mathbf{N} = \nabla d / |\nabla d|$ denotes the outward unit normal to the fracture surface, h_e is the characteristic discretization size, and $\mathbf{I}$ is an identity tensor. Thus, following [7, 1], the fluid equation involve pressure files read

$$\boxed{\frac{\dot{p}}{M} + B\dot{J} - \bar{r}_F + \text{Div}[\mathcal{F}] = 0\ .} \tag{8}$$

2.1.2 Fracture contribution

The crack driving state function in the regularized sense conjugate to crack phase-field denoted as $D(\boldsymbol{\varphi}, d, \mathbf{x})$ for every point $\mathbf{x}$ in domain act as a driving force for the fracture evolution state reads

$$D(\boldsymbol{\varphi}, d, \mathbf{x}) := \frac{2l}{G_c}(1 - \kappa)\psi_{\text{elas}}(\mathbf{F}). \tag{9}$$

Here, G_c is the Griffith's critical elastic energy release rate, and $l = 2h_e$ is the regularization term. Following [6], the local evolution of the crack phase-field equation in the given domain $\mathcal{B}$ results in the third Euler-Lagrange differential system as

$$\boxed{(1 - d)\mathcal{H} - [d - l^2\Delta d] = \eta\dot{d} \quad in\ \mathcal{B},} \tag{D}$$

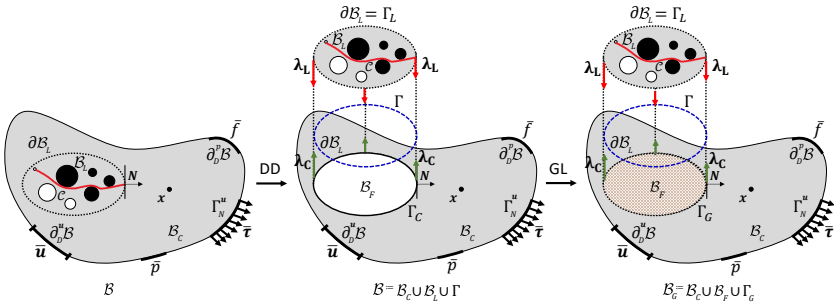

Fig. 2 Configuration and loading setup of the single-scale BVP (left). Middle/right: global-local configuration, by the fictitious domain $\mathcal{B}_F$ through filling the gap between $\mathcal{B}_C$ and $\mathcal{B}_L$ with a same constitutive modeling and discretization of $\mathcal{B}_C$ such that its unification is a so-called global domain $\mathcal{B}_G := \mathcal{B}_C \cup \Gamma_G \cup \mathcal{B}_F$.

augmented by the homogeneous Neumann boundary condition that is $\nabla d \cdot \mathbf{n} = 0$ on $\partial\mathcal{B}$, with the maximum absolute value for the crack driving state $\mathcal{H} = \max_{s\in[0,t]} D(\boldsymbol{\varphi}) \geq 0$ to avoid irreversibly. For different approach see [8]. Thus, following our recent work [11], the variational formulations for the three PDEs for the coupled poroelastic media of the fracturing material are

$$
\begin{aligned}
\mathcal{E}_{\varphi}(\mathfrak{U}, \delta\boldsymbol{\varphi}) &= \int_{\mathcal{B}} \Big[\mathbf{P} : \nabla\delta\boldsymbol{\varphi} - \bar{\mathbf{b}} \cdot \delta\boldsymbol{\varphi} \Big] dV - \int_{\partial_N \mathcal{B}} \bar{\boldsymbol{\tau}} \cdot \delta\boldsymbol{\varphi} \; dA = 0 \,, \\
\mathcal{E}_{p}(\mathfrak{U}, \delta p) &= \int_{\mathcal{B}} \Big[\Big(\frac{1}{M}(p - p_n) + B(J - J_n) - \Delta t \; \bar{r}_F \Big) \delta p + (\Delta t \; \mathbf{K} \; \nabla p) \cdot \nabla\delta p \Big] dV \\
&\quad + \int_{\partial_N \mathcal{B}} \bar{f} \; \delta p \; dA = 0 \,, \\
\mathcal{E}_{d}(\mathfrak{U}, \delta d) &= \int_{\mathcal{B}} \Big[\Big(2\psi_c \; d + 2(d-1)\mathcal{H} \Big) \delta d + 2\psi_c \; l^2 \; \nabla d \cdot \nabla\delta d \Big] dV = 0 \,.
\end{aligned}
\tag{10}
$$

This set of equation is now written in the abstract form through $\mathtt{SS}(\mathfrak{U})$.

3 Multiscale modeling via a non-intrusive global-local method

The previously introduced system of equations for single-scale analysis in (10) for the coupled problem of poroelasticity and fracture is further extended towards the global-local (GL) method now. Following [1, 5], the GL formulation is rooted in domain decomposition (e.g., [12]) by distinguishing the original domain into coarse and fine discretizations, see Figure 2. To couple the domains, namely global and local domains, we have introduced an additional auxiliary interface denoted as Γ between two disjoint domains in poroelastic media (see [1]), and thus corresponding unknown fields, see Figure 2. These additional fields are the interface deformation $\boldsymbol{\varphi}_\Gamma(\mathbf{x}, t)$ and pressure $p_\Gamma(\mathbf{x}, t)$ on auxiliary interface and their corresponding traction forces $\{\boldsymbol{\lambda}^{\boldsymbol{\varphi}}_L, \boldsymbol{\lambda}^{\boldsymbol{\varphi}}_C\}$ and $\{\lambda^{p}_L, \lambda^{p}_C\}$ that are introduced as Lagrange multipliers. These results in a set of coupling equations at the interface by

$$
\begin{cases}
\boldsymbol{\varphi}_L(\mathbf{X}, t) = \boldsymbol{\varphi}_\Gamma(\mathbf{X}, t) & \text{at } \mathbf{X} \in \Gamma_L, \\
\boldsymbol{\varphi}_G(\mathbf{X}, t) = \boldsymbol{\varphi}_\Gamma(\mathbf{X}, t) & \text{at } \mathbf{X} \in \Gamma_G, \\
\boldsymbol{\lambda}^{\boldsymbol{\varphi}}_L(\mathbf{X}, t) + \boldsymbol{\lambda}^{\boldsymbol{\varphi}}_C(\mathbf{X}, t) = \boldsymbol{0} & \text{at } \mathbf{X} \in \Gamma,
\end{cases}
\quad \text{and} \quad
\begin{cases}
p_L(\mathbf{X}, t) = p_\Gamma(\mathbf{X}, t) & \text{at } \mathbf{X} \in \Gamma_L, \\
p_G(\mathbf{X}, t) = p_\Gamma(\mathbf{X}, t) & \text{at } \mathbf{X} \in \Gamma_G, \\
\lambda^{p}_L(\mathbf{X}, t) + \lambda^{p}_C(\mathbf{X}, t) = 0 & \text{at } \mathbf{X} \in \Gamma.
\end{cases}
\tag{11}
$$

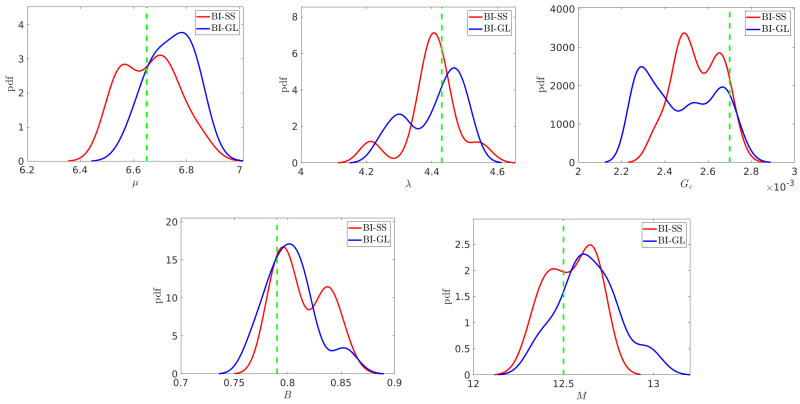

Fig. 3 The pdf of posterior density of the material parameters using the BI-GL and BI-SS approaches for fracture. The true values are shown with a dashed green line.

Now, the multi-physics problem for the global-local approach is described through eleven primary fields to characterize the hydro-poro-elasticity of fluid-saturated porous media at finite strains by

$$\text{Extended Primary Fields}: \mathfrak{P} := \{\boldsymbol{\varphi}_G, \boldsymbol{\varphi}_L, p_G, p_L, d_L, \boldsymbol{\lambda}_C^{\mathbf{u}}, \boldsymbol{\lambda}_L^{\mathbf{u}}, \lambda_C^p, \lambda_L^p, \mathbf{u}_\Gamma, p_\Gamma\} \ . \quad (12)$$

Herein, a global constitutive model behaves as a poroelastic response, abbreviated as E(elastic)-P(pressure), which is augmented with a *single local domain* and behaves as a poroelastic material with fracture response, abbreviated as E(elastic)-P(pressure)-D(damage). The resulting final algorithm is based on our prior work [1, 11].

4 Bayesian inversion for parameter estimation

In this study, we use MCMC (Markov chain Monte Carlo) techniques to identify the material parameters in the hydraulic porous medium phase-field fracture setting. The latter is solved with the previously described GL approach. In general, we can employ the following probabilistic model to update the available prior information according to the forward model (here considers the phase-filed fracture) and a reference observation (arising from measurement, or a synthetic observation). First, we introduce the following statistical model

$$\mathbb{M} = \mathcal{P}(\boldsymbol{x}, \chi) + \varepsilon. \quad (13)$$

Here $\mathbb{M}$ refers to the reference observation arising from the experimental data (a measured value) and $\mathcal{P}$ considers to the model response related to χ a set of d-dimensional material parameters. Furthermore, $\boldsymbol{x} \in \mathbb{R}^\delta$ and ε indicates the measurement error. It is assumed to have Gaussian independent and identically distributed error $\varepsilon \sim \mathcal{N}(0, \sigma^2 I)$, having the parameter σ^2. Since $\mathcal{P}$ in (13) is a model response which results in our computation, such that in our presented model can be approximated through

$$\texttt{signle-scale:} \quad \mathcal{P} \approx \mathcal{P}^{\mathrm{SS}} \quad \text{or} \quad \texttt{global-local:} \quad \mathcal{P} \approx \mathcal{P}^{\mathrm{GL}},$$

corresponds to equations (SS) and (GL), respectively. Thus, (13) becomes as

$$\mathcal{M} = \mathcal{P}^\bullet(\Theta) + \varepsilon, \quad \text{with} \quad \bullet \in \{\mathrm{SS},\mathrm{GL}\}. \quad (14)$$

Despite the simplicity of the Metropolis-Hastings algorithm, it is not suitable for complicated cases, specifically when several parameters should be estimated (multi-dimensional domains). In this study, we use MCMC with ensemble-Kalman filter, see for a detailed discussion [11]. The ensemble Kalman filter (EnKF) indicates the error covariance matrix by a large random ensemble of model observations. Here, to achieve a reliable estimation of posterior density, a Kalman gain is computed using the mean and the covariance of the prior density and the cross-covariance between material parameters and observations. Using an ensemble-Kalman filter, we adopt the proposal density with $\chi^{\star} = \chi^{j-1} + \Delta\chi$, where $\Delta\theta$ is the jump of Kalman-inspired proposal. Afterwards, we update the candidate via $\Delta\chi = \mathcal{K}\left(y^{j-1} + s^{j-1}\right)$. The Kalman gain is computed by $\mathcal{K} = C_{\theta M}\left(C_{MM} + \mathcal{R}\right)^{-1}$, where $C_{\theta M}$ is the covariance matrix between the unknowns and the model response, C_{MM} denotes the covariance matrix of the PDE-based model, and $\mathcal{R}$ is the measurement noise covariance matrix [13]. Moreover, y^{j-1} is the residual of candidates w.r.t the model and $s^{j-1} \sim \mathcal{N}(0, \mathcal{R})$ relates to the density of measurement. Denoting `obs` as an observation, $y^{j-1} = \texttt{obs} - f(\theta^{j-1})$. We refer the reader to [9] for more details and the codes.

Thus, we are now able to use Bayesian inversion to identify the fracking process using multiscale approach material parameters that cannot be measured with usual techniques.

5 Numerical example

In this section, we investigate a numerical test with the main goal that Bayesian inversion yields accurate parameter identifications at a cheap cost of the governing global-local phase-field solver. The mechanical and geomechanical descriptoion of the parameters is given in [10]. In the following, a BVP is applied to the square plate shown in Figure 4. The geometry and boundary conditions are from [1]. The single-scale (SS) model results considering the phase-field and pressure are given in Figure 5. Then, we employ our global-local approach, with findings shown in Figure 6. Figure 7 shows the load-displacement curve for both approachs, indicating the accuracy of the GL approach. Finally, the computational costs of both approaches using the Bayesian setting is given in Table 1, denoting the significant efficiency of the domain decomposition technique.

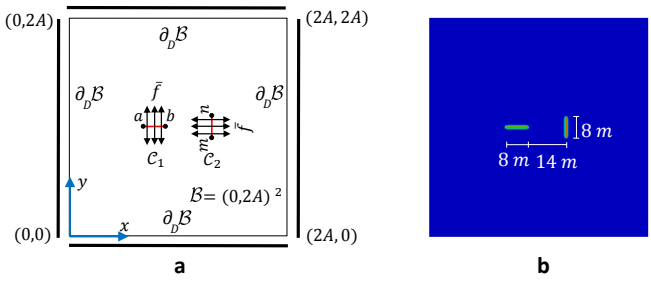

Fig. 4 Joining of two cracks driven by fluid volume injection. (a) Geometry and boundary conditions; and (b) described crack phase-field d as a Dirichlet boundary conditions at $t = 0\ s$.

6 Conclusion

In this study, we extended a global-local (GL) approach for phase-field fracture as the PDE-based model with Bayesian inversion. We applied the proposed idea to hydraulic fracturing within poromechanics concepts, for materials undergoing large deformations. For our numerical example, Bayesian inversion using GL is 20 times faster than the signle-scale model, while the accuracy is similar.

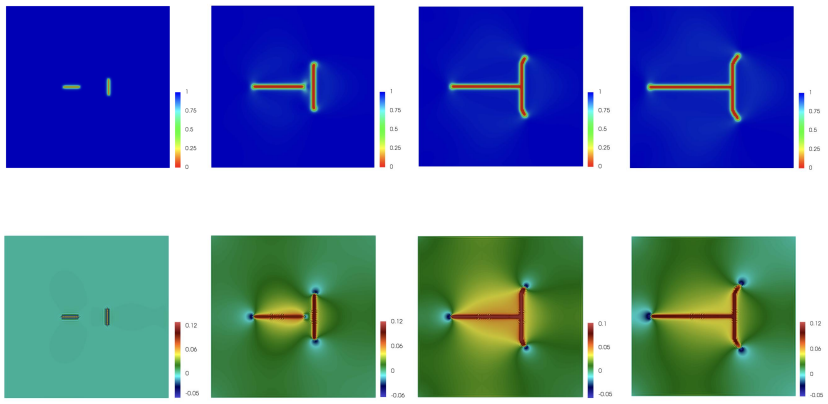

Fig. 5 The evolution of the phase-field (first line) and pressure (second line) for different fluid injection time, i.e., $t \in [0.1, 10, 15, 20]$ seconds using SS model.

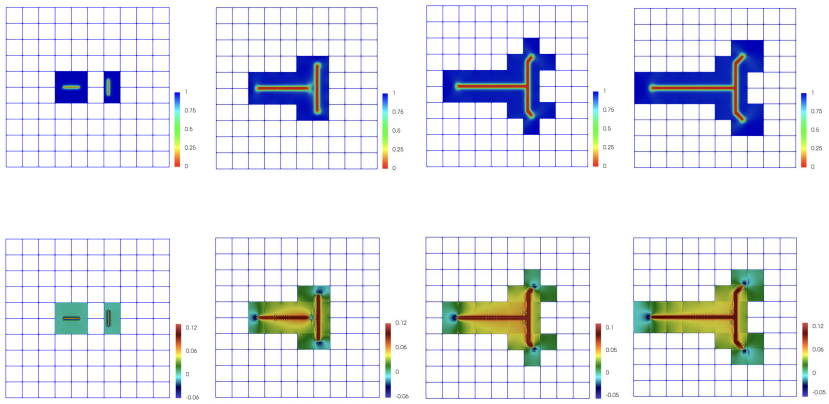

Fig. 6 The evolution of the phase-field (first line) and pressure (second line) for different fluid injection time, i.e., $t \in [0.1, 10, 15, 20]$ seconds using GL model.

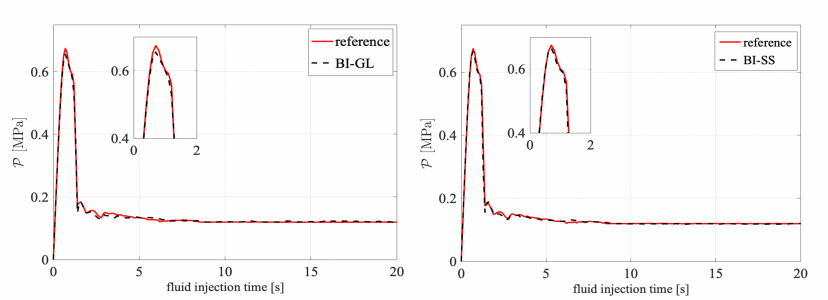

Fig. 7 A comparison between the maximum pressure obtained by the true values (the reference observation) and the mean value of posterior density of BI-GL (left) and BI-SS (right).

Table 1 A comparison between the computational costs of BI-SS and BI-GL approaches for hydraulic fracture. The unit is given in seconds.

Model	min T	max T	mean T	$\sum T$	ratio T
BI – SS	5 645	5 767	5 704	1.14×10^6	19.47
BI – GL	277	296.2	287.1	5.75×10^4	–

Acknowledgements N. Noii acknowledges the Priority Program Deutsche Forschungsgemeinschaft DFG-SPP 2020 within its second funding phase. T. Wick and A. Khodadadian acknowledge the DFG under Germany Excellence Strategy within the Cluster of Excellence PhoenixD (EXC 2122, Project ID 390833453.

References

1. Aldakheel, F., Noii, N., Wick, T., and Wriggers, P. A global–local approach for hydraulic phase-field fracture in poroelastic media. *Computers & Mathematics with Applications* **91**, 99–121 (2021).
2. Bourdin, B., Francfort, G., and Marigo, J.-J. Numerical experiments in revisited brittle fracture. *Journal of the Mechanics and Physics of Solids* **48**(4), 797–826 (2000).
3. Francfort, G. and Marigo, J.-J. Revisiting brittle fracture as an energy minimization problem. *Journal of the Mechanics and Physics of Solids* **46**(8), 1319–1342 (1998).
4. Gendre, L., Allix, O., Gosselet, P., and Comte, F. Non-intrusive and exact global/local techniques for structural problems with local plasticity. *Computational Mechanics* **44**, 233–245 (2009).
5. Gerasimov, T., Noii, N., Allix, O., and De Lorenzis, L. A non-intrusive global/local approach applied to phase-field modeling of brittle fracture. *Advanced Modeling and Simulation in Engineering Sciences* **5**(1), 14 (2018).
6. Miehe, C., Hofacker, M., Schänzel, L.-M., and Aldakheel, F. Phase field modeling of fracture in multi-physics problems. Part II. Coupled brittle-to-ductile failure criteria and crack propagation in thermo-elastic–plastic solids. *Computer Methods in Applied Mechanics and Engineering* **294**, 486–522 (2015).
7. Miehe, C. and Mauthe, S. Phase field modeling of fracture in multi-physics problems. part iii. crack driving forces in hydro-poro-elasticity and hydraulic fracturing of fluid-saturated porous media. *Computer Methods in Applied Mechanics and Engineering* **304**, 619–655 (2016).
8. Noii, N., Fan, M., Wick, T., and Jin, Y. A quasi-monolithic phase-field description for orthotropic anisotropic fracture with adaptive mesh refinement and primal–dual active set method. *Engineering Fracture Mechanics* **258**, 108060 (2021).
9. Noii, N., Khodadadian, A., Ulloa, J., Aldakheel, F., Wick, T., Francois, S., and Wriggers, P. Bayesian inversion with open-source codes for various one-dimensional model problems in computational mechanics. *Archives of Computational Methods in Engineering* **29**(6), 4285–4318 (2022).
10. Noii, N., Khodadadian, A., and Wick, T. Bayesian inversion for anisotropic hydraulic phase-field fracture. *Computer Methods in Applied Mechanics and Engineering* **386**, 114118 (2021).
11. Noii, N., Khodadadian, A., and Wick, T. Bayesian inversion using global-local forward models applied to fracture propagation in porous media. *International Journal for Multiscale Computational Engineering* **20**(3) (2022).
12. Toselli, A. and Widlund, O. *Domain decomposition methods-algorithms and theory*, vol. 34. Springer Science & Business Media (2004).
13. Zhang, J., Vrugt, J. A., Shi, X., Lin, G., Wu, L., and Zeng, L. Improving Simulation Efficiency of MCMC for Inverse Modeling of Hydrologic Systems with a Kalman-Inspired Proposal Distribution. *Water Resources Research* **56**(3), e2019WR025474 (2020).